J Nanopart Res (2018) 20: 10
https://doi.org/10.1007/s11051-017-4110-5

RESEARCH PAPER

Synthesis, photoelectrochemical properties and solar light-induced photocatalytic activity of bismuth ferrite nanoparticles

Sambhu Prasad Pattnaik · Arjun Behera · Satyabadi Martha · Rashmi Acharya · Kulamani Parida

Received: 12 September 2017 / Accepted: 15 December 2017 / Published online: 6 January 2018

Abstract Bismuth ferrite (BFO) nanoparticles prepared by solid state reaction route were characterized by various characterization techniques such as XRD, FESEM, HRTEM, UV–Vis DRS, PL etc., and their photocatalytic activities were evaluated by decolorization of aqueous solution of Congo red (CR) under solar light. The photocatalytic activity of BFO was increased by increasing the preparation temperature from 350 to 500 °C and then decreased with rise in temperature. The results of electrochemical measurements such as linear sweep voltammetry (LSV), electrochemical impedence (EIS), and Mott–Schottky analysis of BFO nanoparticles corroborated the findings of their photocatalytic activity. The enhanced photocatalytic response of the sample prepared at 500 °C is attributed to its smallest band gap, minimum crystallite size (30 nm), efficient separation, and lowest possible recombination of photo-generated charge carriers. The effects of amount of nano-BFO, irradiation time, initial CR concentration, and BFO calcination temperature on the decolorization of CR were examined. It was observed that 1 g/L nano-BFO calcined at 500 °C can decolorize up to 77% a 10-ppm CR dye solution under solar irradiation for 60 min. The studies included scavenger tests for identification of reactive species and a possible mechanism of dye decolorization.

S. P. Pattnaik (✉) · A. Behera · S. Martha · R. Acharya · K. Parida (✉)
Centre for Nano Science and Nano Technology, ITER, Siksha 'O' Anusandhan University, Bhubaneswar, Odisha 751030, India
e-mail: sp1pattnaik@gmail.com
e-mail: kulamaniparida@soauniversity.ac.in

Keywords BFO · Photocatalysis · Solid-state reaction bismuth ferrite · Photoelectrochemical properties · Congo red decolorization · Energy conversion

Introduction

Photocatalytic decolorization of pollutants and photocatalytic water splitting for production of hydrogen are two widely used clean and environment friendly techniques to solve environmental and energy problems (Kandi et al. 2017; Nayak et al. 2015; Patnaik et al. 2016). Semiconductor based photocatalysts such as TiO_2, SnO_2, and ZnO have been considered as efficient materials for this purpose because of their excellent photocatalytic activity, high chemical stability, non-toxicity, and low cost (Jing et al. 2013). However, these oxide semiconductors possess wide-band gap and can only absorb about 5% of sunlight in the ultraviolet region, which obviously restricts their practical usefulness. Therefore, it is very essential to develop visible light-driven photocatalysts for the photo degradation of organic pollutants.

Recently, multiferroic materials are utilized in both photocatalysis and photovoltaics due to their narrow energy band gaps and ferroelectric properties, which permit them to absorb light mostly in the visible region (Choi et al. 2009; Nechache et al. 2011; Gao et al. 2006; Joshi et al. 2008). Perovskite bismuth ferrite (BFO) is the only known room temperature multiferroic material with high Curie temperature ($T_c \approx 1100$ K) and G-type antiferromagnetic order below the Neel temperature

($T_N \approx 643$ K) (Wang et al. 2003). BFO is also being recognized as a newly emerging visible light active photocatalyst for both pollutant decolorization and water splitting because of its high chemical stability, suitable band gap, ferroelectric, and ferromagnetic properties (Gao et al. 2007; Li et al. 2010; Gao et al. 2014). Moreover, its ferroelectric properties with spontaneous polarization lead to the band bending that mobilizes the photo-generated electrons and holes in opposite directions, resulting in efficient separation of these charge carriers, which enhances the photocatalytic activity (Quinonez et al. 2013).

The study of photocatalytic activity of BFO nanoparticles towards effective degradation of dyes under visible light irradiation targeting future treatment of aqueous effluents from textiles industries is continued to attract the interest of researchers to this day. A few of such recent studies using BFO nanoparticles under visible light are mentioned as under. Researchers studied degradation of dyes like methyl orange (MO) (Gao et al. 2007), rhodamine B (RhB) (Wang et al. 2011) and methylene blue (MB) (Jiang et al. 2011) using BFO nanophotocatalyst.

The degradation of RhB, MB, and reactive black 5 (RB5) has been studied by using BFO synthesized via sonochemical route (Soltani and Mohammad 2013; Soltani and Entezari 2013a, b). The degradation of MB and RhB, under the simulated solar light irradiation using BFO nanofibers was investigated (Bharathkumar et al. 2016).The degradation of methyl violet (MV) (Dhanalakshmi et al. 2016) and that of RhB (Bai et al. 2016) were studied using BFO as photocatalyst.

Further, the photocatalytic activity is influenced by the particle size, surface morphology, and crystallinity of a photocatalyst. In order to get BFO particles of desired particle size and morphology, several preparation methods such as solid-state reaction (Wang et al. 2004; Kumar et al. 2000), sol-gel (Rashad 2012), hydrothermal (Tsai et al. 2012), etc. have been employed. Among these techniques, solid-state reaction method is the simplest, convenient, and economic one that requires less chemicals and minimum time for preparation. Single-phase polycrystalline BFO particles were synthesized by subjecting a mixture of Bi_2O_3 and Fe_2O_3 at 880 °C for a short time of 450 s (Valant et al. 2007). BFO ceramic samples were synthesized by a rapid liquid phase sintering technique and their magnetic and ferroelectric behaviors have been studied (Wang et al. 2003). However, the photoelectrochemical measurements and photocatalytic activity evaluation of BFO samples together have rarely been reported.

In this work, BFO nanoparticles were synthesized by solid-state reaction method at different temperatures and their photocatalytic activity was evaluated by decolorization of CR under irradiation of solar light. Different photoelectrochemical measurements such as photoluminescence, electrochemical impedence (EIS), linear sweep voltametry (LSV), and Mott–Schottky analysis were carried out to explore the possible reasons for variation in photocatalytic activity among BFO nanoparticles. Further, effect of preparation temperatures, amount of photocatlysts, irradiation time, and initial concentration of dye solution on photocatalytic activity of BFO were studied. The role of superoxide free radicals (O_2) on decolorization process are investigated by using disodium salt of ethylene diamine tetra-acetic acid (EDTA-2Na), dimethyl sulfoxide (DMSO), isopropyl alcohol, and p-benzoquinone as scavenging agents. Based on these, a proposed mechanism on photocatalytic activity of BFO nanoparticles towards decolorization of CR is presented.

Experimental

Materials

All the reagents were of analytical grade and used in the reaction without any further purification.

Synthesis of bismuth ferrite nanoparticles

BFO nanoparticles were prepared by solid-state reaction method. At first, equimolar mixture of $Bi(NO_3)_3.5H_2O$ (5.15 g) and $Fe(NO_3)_3.9H_2O$ (4.12 g) were thoroughly ground and intimately mixed for about half an hour by means of a mortar and pestle. The prepared mixture was annealed at different temperatures ranging from 350 to 800 °C for 4 h in a furnace at a heating rate of 5 °C per minute. The annealed material was finely ground, homogenized, kept in a sealed container, and labeled. The bismuth ferrite samples annealed at 350, 400,500,600,700, and 800 °C are named as BFO350, BFO400, BFO500, BFO600, BFO700, and BFO800, respectively.

Characterization

The prepared products were characterized by different instrumental techniques. XRD patterns of all the samples were obtained on Rigaku Miniflex(set at 30 kV and 15 mA) diffractometer using Cu Kα radiation ($\lambda = 1.54$ Å). The SEM images were observed on a Zeiss Supra 55 scanning electron microscope at an accelerated voltage of 20 kV. The electron micrographs of the samples were recorded by a transmission electron microscope (TEM) JEOL JEM-2010 at an accelerating voltage of 200 kV. The UV–Vis diffuse reflection spectra (UV–Vis DRS) of BFO samples were measured with a JASCO V-750 spectrophotometer in order to study optical absorption property. The scan was conducted over a spectral range of 200 to 800 nm with boric acid as reference. The PL spectral measurements were carried out at room temperature with excitation at 320 nm on a scanning JASCO FP 8300 spectrofluorometer using a solid sample attachment.

Photoelectrochemical measurements

The photoelectrochemical measurements were carried out by a multichannel electrochemical analyzer (IVIUMn STAT) provided with three-electrode system using 100 ml of 0.1 M Na_2SO_4 solution of pH 6.8 as electrolyte at 25 °C under dark and illumination conditions. The cell of the three-electrode system consisted of a BFO film electrode, Ag/AgCl, and Pt electrode as working electrode (photo-anode), reference electrode, and counter electrode (cathode), respectively. The working electrodes were prepared by following procedure. fluorine doped tin oxide (FTO) electrodes were washed with acetone, ethanol, and deionized water several times by ultrasonic technique. Twenty milligrams each of iodine and BFO powder were dispersed in 40 mL of acetone and were sonicated for 10 min. BFO films were then coated on FTO by electrophoresis method, and the active area of electrodes were controlled to be (1.0×1.0 cm^2). The coated FTOs were dried in a vacuum oven at concentration 60 °C for 24 h to get desired electrodes. The working electrodes were illuminated with a Xenon lamp (300 W) equipped with a UV cut-off filter ($\lambda \geq 400$ nm). EIS were recorded under visible light ($\lambda \geq 400$ nm) irradiation by applying an AC voltage of 5 mV in the frequency range from 0.01 Hz to 100 kHz. The Mott–Schottky plot was obtained using frequency of 1500 Hz.

Photocatalytic activity

The photocatalytic activities of the BFO samples were evaluated by the photo-decolorization of Congo red (CR) in an aqueous solution under solar light irradiation. Experiments were conducted in stoppered 100 mL conical flasks for 60 min by varying the concentration of BFO from 0.5 to 2.0 gL^{-1} and initial concentration of CR solution from 5.0 to 50.0 mg L^{-1}. The BFO suspension was magnetically stirred in dark for half an hour before irradiation of solar light. After completion of experiments, the suspension was centrifuged at a speed of 8000 rpm for 10 min. The supernatant solutions were taken to measure the residual concentration of CR with the help of a JASCO V-750 UV–Vis spectrophotometer at 497 nm. All the experiments were carried out in triplicate during the hot summer days from 10.00 am to 11.00 am. The average luminosity during the experiments is found to be 102,000 lx. The percentage of decolorization (DE) was calculated as per Eq. 1.

$$\%DE = 100 \text{ x } (C_0 - C)/C_0 \quad (1)$$

where, C_0 and C are initial and final concentration of the CR solution, respectively.

The influence of active species in the photocatalytic decolorization process was studied by different scavengers like disodium salt of EDTA-2Na, dimethyl sulfoxide (DMSO), p-benzoquinone (BQ), and isopropyl alcohol for trapping of holes, electrons, super oxide radicals, and hydroxyl radicals, respectively. In order to determine the active species responsible for decolorization, experiments were carried out under controlled conditions by using various scavengers.

The best BFO photocatalyst was studied for reusability as per the following procedure. After completion of every decolorization test the photocatalyst was separated by centrifugation, washed thrice with double-distilled water followed by three times ethanol wash and dried in the oven. The sample so obtained was reused in second test and this procedure was repeated again under similar test conditions for third time to check the stability and reusability of the BFO photocatalyst.

Results and discussions

Formation and characterization of bismuth ferrite

The XRD patterns of BFO samples were shown in Fig.1. The XRD patterns confirmed the formation of perovskite Bismuth ferrite corresponding to JCPDS card no. 73-0548 and revealed the rhombohedral crystal structure of BiFeO3 phase. As shown, the intensity of the most prominent peak of BFO at 32.04° indexed as (110) diffraction plane found to be increasing with annealing temperature and highest for sample annealed at 800 °C.

This is expected as the crystallinity of perovskite structure improved with calcination temperature. The same peak was found to be broad for 500 °C sample implying formation of nano-sized particles (Martha et al. 2012a, b). The average crystallite size of different samples were determined from XRD data using Scherer's equation (Langford and Wilson 1978; Ahmad et al. 2012) and plotted against calcination temperature as shown in Fig. 2. The smallest size nanoparticles of 30 nm were obtained from samples calcined at 500 °C and the samples calcined at 800 °C yielded large sized particles (about twice the minimum size) of 67 nm. The crystallite size decreased progressively when calcination temperature increased from 350 to 500 °C and thereafter increased as the temperature varied from 500 to 800 °C and the average crystallite size of nanoparticles (NPs) as calculated by X-ray diffraction (XRD falls in the range of 30–67 nm. The crystallite size changed due to agglomeration and compaction of BFO nanoparticles with variation in temperature (Martha et al. 2012a, b).

The clear and distinct XRD peaks of BFO particulates indicated their enhanced crystalline nature, while the broadened XRD peaks of BFO500 particles represented reduced crystallite size 30 nm of the particulates. This can also be corroborated with the calculated crystallite sizes from Scherer's formula (Ahmad et al. 2012).

The BFO prepared by solid-state reactions have generated a small amount of easily forming impurities (Moitra et al. 2016) due to kinetics of formation during synthesis (Dhanalakshmi et al. 2016). They are manifested as weak XRD peaks between 26.5 to 29° and could be seen for all the BFO samples calcined at different temperatures. The impurity peaks may be due to presence of $Bi_2Fe_4O_9$ and $Bi_{25}FeO_{40}$ (Peng et al. 2011).

The well crystalline character of BFO500 nanoparticles is responsible for its better photocatalytic activity compared to other BFO samples annealed at different temperatures.

FESEM micrographs of BFO500 photocatalyst were shown in Fig. 3. The sample was observed to be non-homogeneous in nature and aggregate of staked loose 2D plates of BFO nanoparticles. The particles are observed to be irregular in size of sub- micron range. The formation of loose 2D plates favors the photocatalytic reaction.

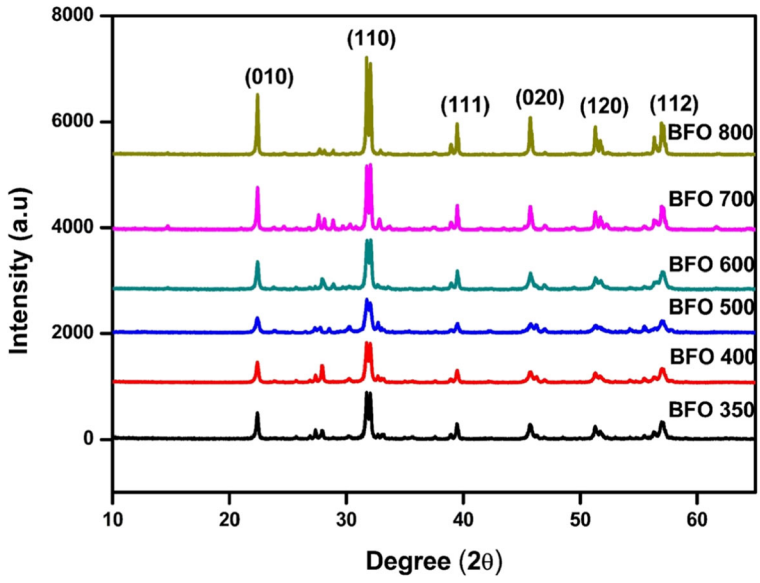

Fig. 1 X-ray diffraction patterns of the prepared bismuth ferrite nanoparticles

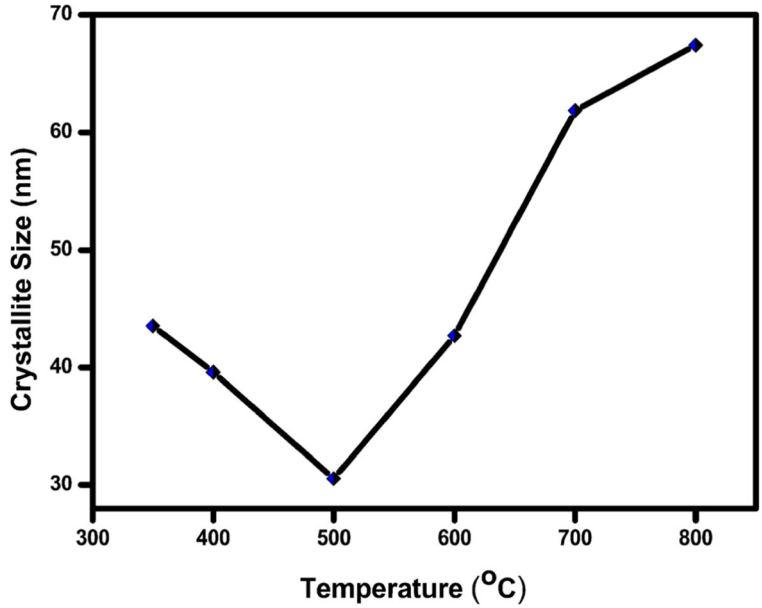

Fig. 2 Variation of crystallite size of BFO nanoparticles with annealed temperatures

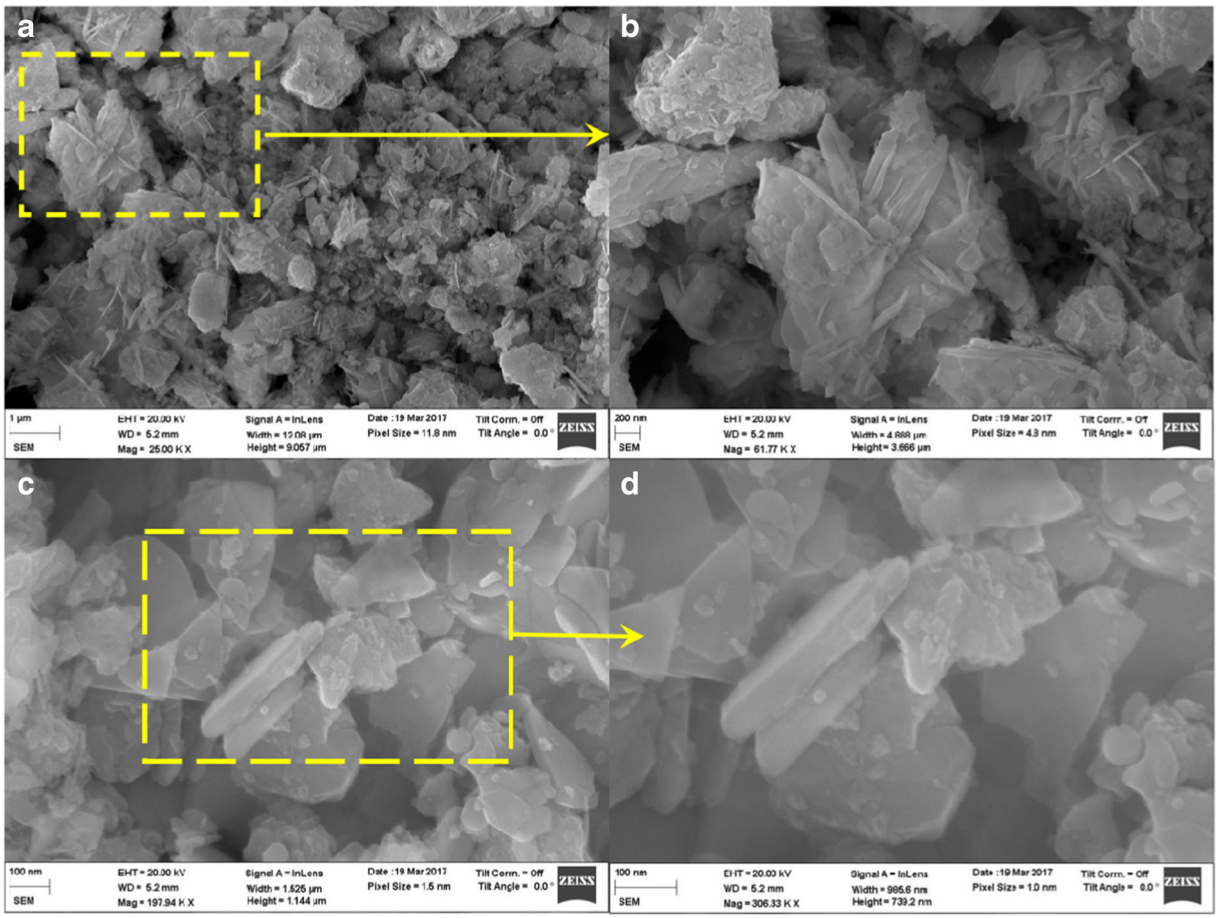

Fig. 3 FESEM micrographs of BFO500 sample

The TEM micrographs of BFO500 photocatalyst are shown in Fig. 4. The agglomerated structure of BFO was observed from TEM micrographs appeared to consist of irregular nanocrystals. The plate like structure observed from TEM micrograph is consistent with SEM. The HRTEM image confirmed the well crystallinity of BFO nanoparticles. The fringes of BFO nanoparticles are separated with each other with a regular interval of 0.28 and 0.396 nm. The above value is well consistent with the d value obtained from XRD data corresponding to the presence of (110) and (010) planes respectively of perovskite BFO. The highly

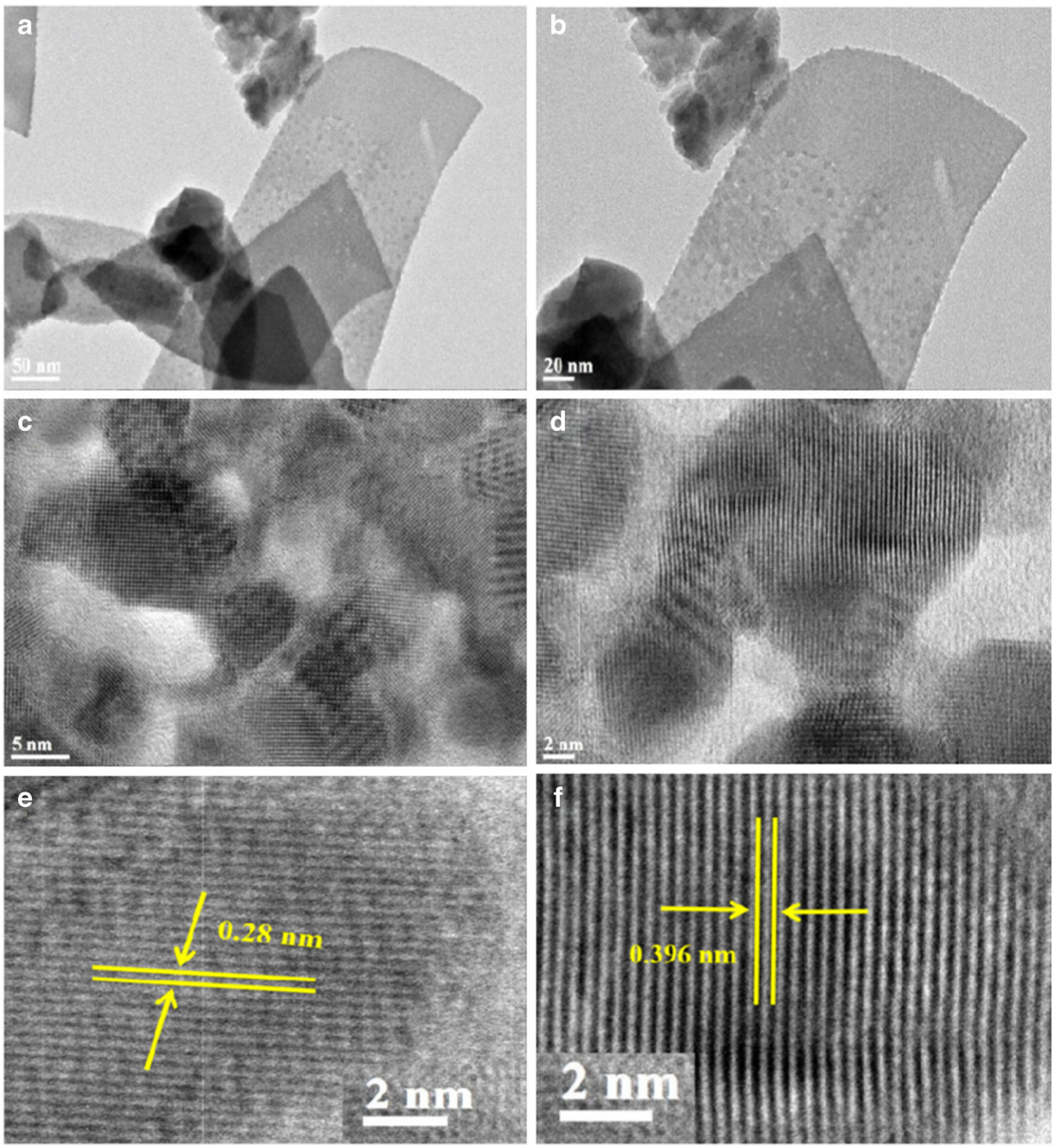

Fig. 4 TEM micrographs of synthesized BFO500 photocatalysts

intense peaks for (110) and (010) planes indicate that the BFO crystallite is preferentially oriented along (110) and (010) planes.

Optical properties

Figure 5a shows the UV–Vis absorption spectrum of synthesized BFO nanoparticles annealed at temperatures ranging from 350 to 800 °C. All the BFO samples annealed at different temperatures were found to absorb light in the visible range from 400 to 800 nm. The magnitude of absorbance values with respect to wavelength of light absorbed indicates that the materials are expected to very active under solar radiation. The highest absorbance was observed for BFO500 sample. With further increase in calcination temperature of samples, the absorbance magnitude decreased as presented in Fig. 5a.

The band gap energy determined from the UV-Vis absorption spectrum of BFO500 sample by drawing a tangent to the spectrum as shown in Fig. 5b and found to be 1.7 eV. The light absorption near band gap for any semiconductor is governed by the following equation,

$$\alpha h\vartheta = C\left(h\vartheta - E_g\right)^n \quad (2)$$

where α, h, ν, E_g, C, and n are absorption coefficient, Planck's constant, light frequency, band gap, and a constant, respectively.

The corresponding direct band gap energy where $n = 2$ is calculated according to the above mentioned equation by plotting the $(\alpha h\nu)^2$vs $(h\nu)$ and extrapolating the linear portion of $(\alpha h\nu)^2$ to the energy $(h\nu)$ axis at $\alpha = 0$ as shown in the inset of 5 (b).After extrapolation, the energy band gap is determined to be 1.8 eV for BFO500 nanoparticles, which is quite comparable with earlier findings (McDonnell et al. 2013). The lower band gap of BFO500 nanoparticles suggests possible utilization of visible light for photocatalysis.

PL study was carried out to study the transfer, relocation and recombination process of the charge carriers (Martha et al. 2014a). Fig. 6 shows the photoluminescence spectra of BFO samples calcined at various temperatures ranging from 400 to 800 °C. The PL spectra of all the synthesized BFO photocatalyst samples were obtained with excitation at 320 nm at ambient temperature. The electron–hole recombination rate may be inferred from the intensity of the PL spectrum. An intense PL spectrum refers to a high rate of electron–hole recombination leading to low photocatalytic activity (Reddy et al. 2013). In this investigation, BFO 800 exhibits the most intense PL peak. Hence it is expected to have maximum recombination rate of electron–holes and consequently exhibit lowest photocatalytic activity.

On the other hand, the lowest intensity of BFO500 photocatalyst sample suggests that mostly photo-excited electrons transferred effectively through the interface of photocatalyst surface and CR solution (Nashim et al. 2013; Martha et al.

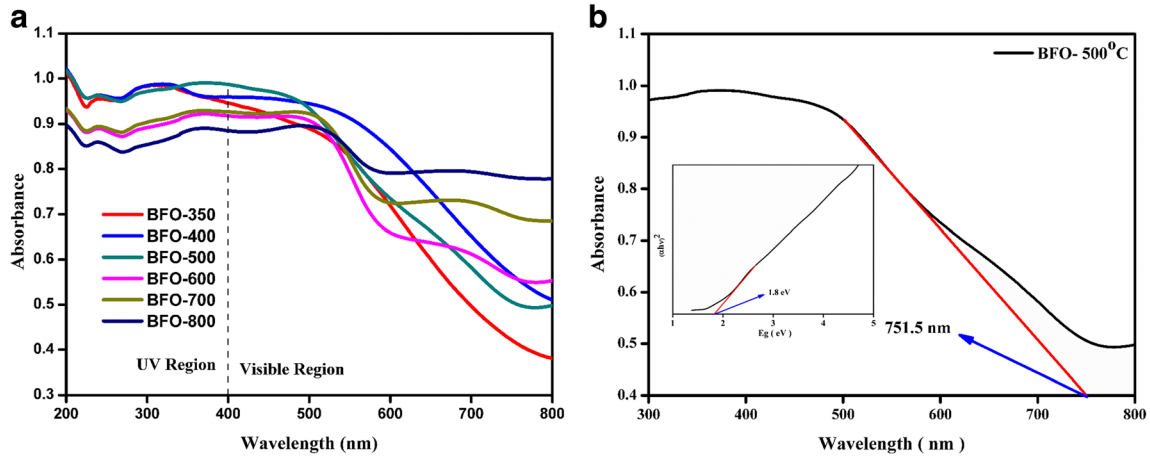

Fig. 5 **a** Diffuse reflectance UV-Vis absorption spectra of bismuth ferrites, **b** UV–Vis absorption spectrum of synthesized BFO500 nanoparticles and the direct band gap estimated from the $(\alpha h\nu)^2$vs $(h\nu)$ plot shown in the inset

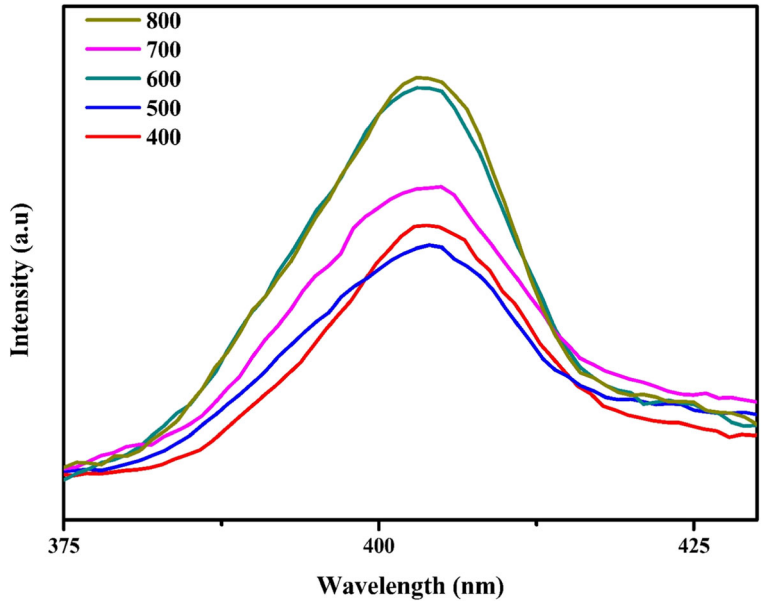

Fig. 6 PL spectra of bismuth ferrite samples annealed at different temperatures

2012a, b). Therefore the probability of recombination of charge carrier in case of BFO500 happens to be minimal. The lowest PL intensity of BFO500 is in line with the lowest particle size obtained from XRD and TEM study. All these observations support that BFO500 exhibits highest photocatalytic activity by minimizing the recombination of charge carriers.

Photoelectrochemical measurements

Linear sweep voltametry (LSV) and photocurrent response

The photocurrent measurement of BFO nanoparticles were carried out under light illumination in 0.1 M Na_2SO_4 solution of pH 6.5 at a scan rate of 20mVs^{-1}. It was observed that the pH of the electrolyte does not change after the photocurrent measurement. This indicates stability of BFO nanoparticles in the electrolytic medium and therefore helpful in case of practical applications. Fig. 7 shows the linear sweep voltammetry (LSV) plots of BFO-350, BFO-400, BFO-500, BFO-600, BFO-700, and BFO-800 under darkness and light illumination respectively. It was evident from the plots that the samples generated anodic current density of 0.1 mA/cm^2 by applying potential of 1.0 V and the current density increases gradually to 1.1 (for BFO800) to 1.8 mA/cm^2 (for BFO500) by increasing the applied potential to 1.5 V in case of different BFO samples under darkness. This anodic current is caused by water oxidation and not due to self-oxidation of the BFO as the latter would have led to photo-corrosion of material and change in pH after electro chemical measurements.

The onset potential under illumination does not change when compared to that in the dark. The onset potential is about 1.1 V (0.8–(− 0.3)) positive than the flatband potential. This difference in potentials may be attributed to mostly poor charge transfer between BFO particles apart from the contribution of over potential due to slow interfacial charge transfer kinetics.

The anodic current density under illumination increased from 0.1 mA/cm^2 at applied potential of 1.0 V to about 3 mA/cm^2 by increasing the applied potential to 1.5 V. Among all BFO samples, the BFO500 generated maximum current density for a given applied potential between 1.0 to 1.5 V. This confirms prepared BFO photoelectrodes are of n-type semiconductor (Li et al. 2004). The photocurrent density for n-type semiconductor depends upon the concentration of electrons and as current density increases so is the concentration of generated electrons (Martha et al. 2014b). Further, the slope for the plot of BFO500 was found to be maximum suggesting generation of largest amount of photocurrent due to highest concentration of generated electrons. This results in maximum charge separation leading to highest photocatalytic activity. The obtained result is also in good agreement with the PL behavior.

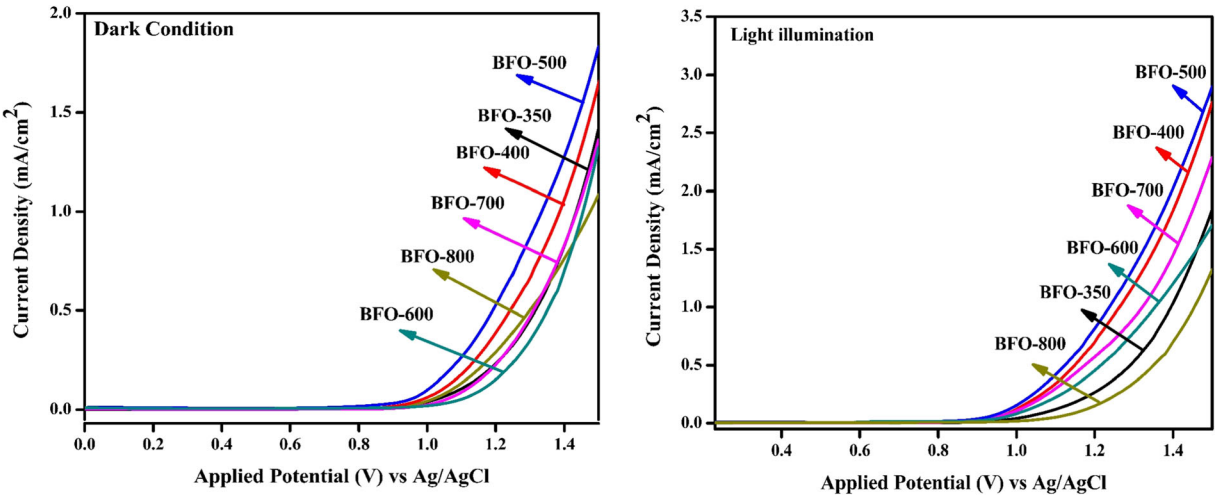

Fig. 7 Current- potential curves of BFO electrodes under dark (left) and illuminated with 300 W Xenon lamp, $\lambda \geq 400$ nm. (right)

Electrochemical impedance spectra

The photocatalytic mechanism, charge transfer resistance and interfacial charge separation efficiency of the prepared BFOs were investigated by EIS as represented by the Nyquist plots. The diameter of Nyquist semicircle is a function of the resistance at the interface between the working electrode and electrolytic solution. It reflects the rate of photocatalytic reaction on the surface of the semiconductor photocatalyst. The smaller diameter is an indicative of faster charge transfer and effective separation of electron–hole pairs, which lead to maximum activity (Martha et al. 2014b). Figure 8 shows the Nyquist plot of BFO samples annealed at different temperatures. It is evident from the figure that the semicircle with smallest diameter is obtained for BFO500 suggesting its lowest resistance for charge transfer and effective charge separation. The effective charge separation process is very much helpful for enhancement of the photocatalytic activity.

Mott–Schottky plot

To investigate the band alignment, analyze the conductivity type and charge transfer process, the Mott–Schottky plots of BFO500 was used (Fig.9). The M-S plot of BFO500 studied under constant frequency revealed negative slope of the line segment suggesting n-type characteristic for BFO500. According to the M-S equation, the flat band potential of BFO500 is calculated. From the X-axis intercept of the linear region of M-S plot and found to be − 0.29 eV. As the prepared BFO is n-type semiconductor, the flat band potential practically coincides with its CB potential (Giannakopoulou et al. 2016; Beranek 2011; Baumanis and Bahnemann 2008) and the same becomes 0.3 eV after converting the potential measurement with respect to R.H.E. From UV-DRS measurement the band gap of BFO was found to be 1.8 eV. So, the valence band VB potential of BFO is be +2.1 eV.

Photocatalytic activities

Photocatalytic activity towards decolorization of Congo red (CR) under solar light irradiation

In order to investigate the photocatalytic activities of prepared BFO photocatalysts, 10 mg L^{-1} of CR solution was decolorized under irradiation of solar light. At first, CR solution of desired concentration was treated under solar light irradiation for 1 h in absence of BFO powders. It was observed that only 1% of CR was decolorized. To explore the possibility of adsorption of CR on to the active sites of the photocatalyst, given CR solution was subjected to stirring in dark for 60 min in presence of 1 g L^{-1} of photocatalyst. Decolorization of about 3% of CR indicated that adsorption of CR onto the BFO photocatalyst is negligible. Then, the photocatalytic activity of BFO samples prepared at different temperatures towards decolorization of CR solution in various time intervals were studied. Figure 10a represents the rate of decolorization of CR solution by prepared BFO photocatalysts.

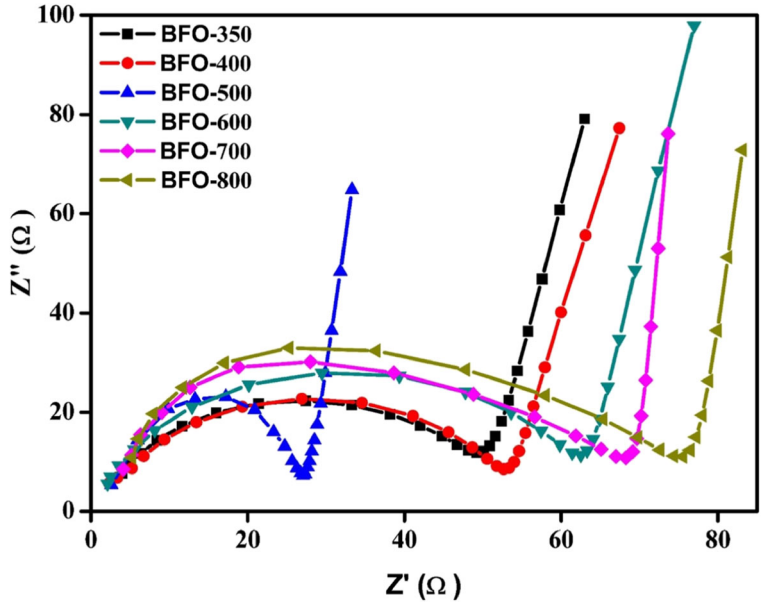

Fig. 8 Nyquist plot for BFO samples annealed at different temperatures

The percentage of decolorization by different BFO photocatalysts decreases in the order BFO500 > BFO400 > BFO600 > BFO700 > BFO800. Maximum 77% of 20 ml of 10 mg L^{-1} CR solution was decolorized by 1.0 g L^{-1} of BFO500 in 60 min. The UV–Vis absorbance spectra of CR with respect to time in presence of BFO500 was shown in Fig. 10b.

It was evident from the figure that the absorption spectra decrease significantly at each time interval of 20 min and found minimum at 60 min. Decrease in concentration of absorption spectra is an indicative of decrease in concentration of CR solution with progress of time which in turn due to the good photocatalytic activity of BFO500. It may be due to its smallest crystallite size as evident from XRD study, which is in agreement with TEM results. Moreover, the lowest PL intensity of the sample suppresses electron-hole pairs' recombination and facilitates their transport for photocatalytic reactions. This enhances the photocatalytic activity of BFO500 and hence maximum percentage of

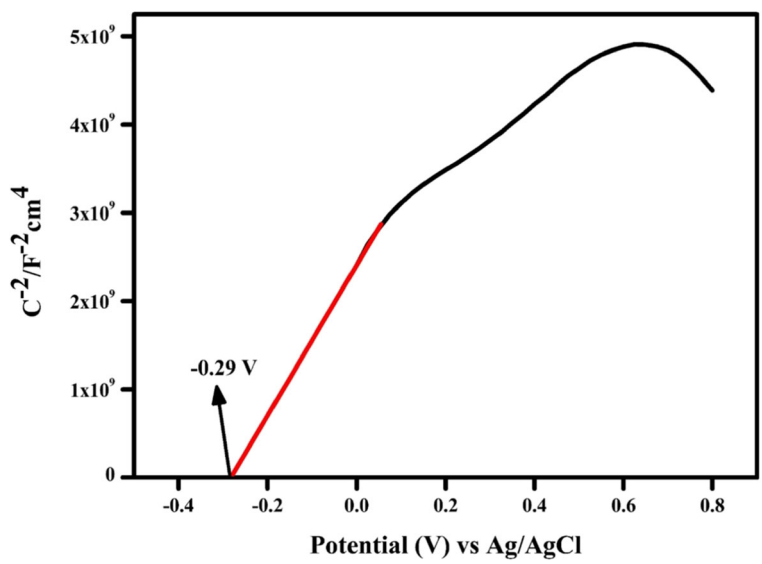

Fig. 9 The Mott–Schottky plot of BFO500 measured with frequency 1500 Hz

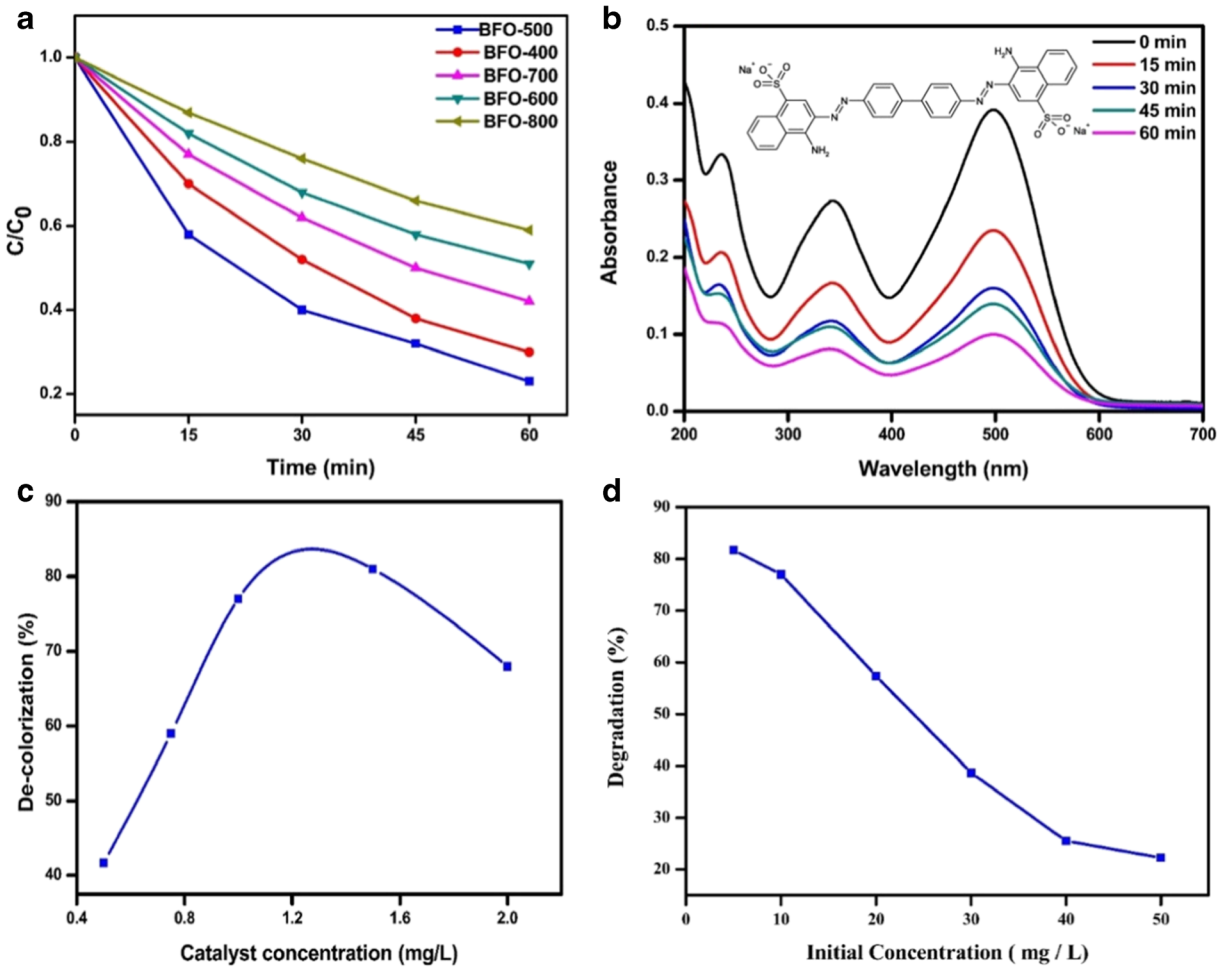

Fig. 10 **a** Effect of annealing temperature of BFO on photo decolorization of CR. Volume of the solution 20 mL, initial concentration of CR10 mg L^{-1}, irradiation time 60 min, pH 6.5. **b** The effect of irradiation time on photo decolorization of CR using BFO500 as photocatalyst. **c** The effect of BFO500 catalyst concentration on photo decolorization of CR. **d** The effect of initial CR concentration on photo decolorization of Congo red using BFO500 as photocatalyst

CR decolorization. Further, electrochemical studies also confirm the lesser recombination of charge carriers and high conductivity of BFO500.

As BFO500 exhibited highest photocatalytic activity towards decolorization of CR, it was used in all photoctalytic reactions carried out further. To investigate the effects of concentration of photocatalyst on CR decolorization, the concentration was varied from 0.5 to 2.0 g L^{-1} keeping other reaction parameters like time, concentration of CR solution, volume of solution, and pH constant. As shown in the Fig. 10c, maximum percentage of decolorization of CR was observed for the solution containing 1.0 to 1.5 g L^{-1} BFO500.

The percentage of CR decolorization increases when the catalyst concentration was increased from 0.5 to 1.5 g L^{-1}. This observation may be due to the increase in available active sites on BFO surface and the amount of light entering into the dispersion (Konstantinou and Albanis 2004). The optimum catalyst concentration for decolorization of CR appears to be 1.0 g L^{-1} as improvement of catalyst concentration further does not increase decolorization efficiency proportionately. Further increase in catalyst concentration from 1.5 to 2.0 g L^{-1} does not improve degradation proportional to increase in catalyst concentration, and at 2.0 g L^{-1} catalyst concentration, it leads to decrease of percentage decolorization of CR. This may be attributed to the increased opacity of the suspension due to excess of BFO particles (Montazerozohori et al. 2007).

The photocatalytic activity of a photocatalyst is also influenced by the initial concentration of dye solution. In order to study the effect of initial concentration of CR solution on percentage of decolorization, different experiments were carried out by varying the concentration from 0.5 to 50 mg L^{-1}. It was observed from the Fig. 10d that the percentage of decolorization decreases slightly from 81 to 77% by increasing initial concentration from 0.5 to10 mg L^{-1}. On further increase of initial concentration resulted in sharp decrease of decolorization rate. This could be attributed to the coverage of CR molecules on the surface active sites of BFO resulting in prohibition of harvesting the solar light by the photocatalyst required for decolorization (Tsai et al. 2012).

The photostability of the BFO500 under visible light irradiation was evaluated by conducting recycling tests. After running every 60 min of photocatalytic reaction in Congo red solution, the separated catalyst was recovered, cleaned, and re-dispersed into the fresh aqueous CR solution. The decrease in concentration of CR during each cycle is shown in Fig. 11. It is seen that after three cycling runs of photodecoloration of CR, the photocatalytic ability of the BFO500 apparently remained same indicating photostability of BFO500.

Mechanism of CR decolorization

Photocatalytic reactions for decompositions of pollutants usually involve production of reactive species like superoxide radical, electron, hydroxyl radical, and hole which decompose the pollutants (Zheng et al. 2009).

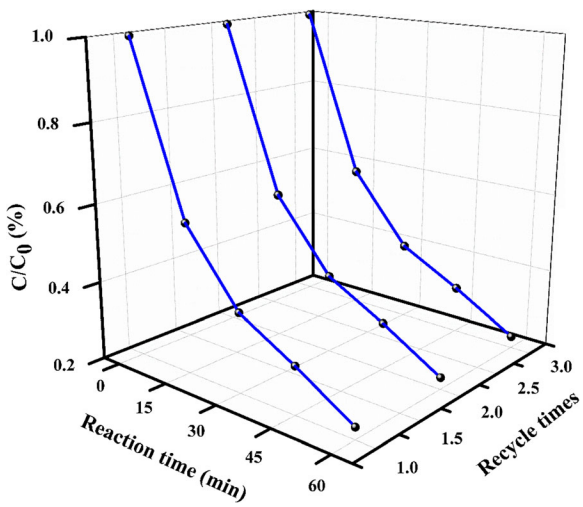

Fig. 11 Photo de-colorization of CR by BFO 500 during the recycle tests. The initial CR concentration was 10 mg/L and the catalyst dose 1.0 g/L

In this study, scavenging agents such as p-benzoquinone (p-BQ), DMSO, IPA, and EDTA were used to identify the reactive species that are involved in photocatalytic decolorization of CR.

The effect of scavenging agents on percentage of decolorization was shown in Fig. 12a. It was evident from the Fig. 12a that percentage of decolorization of CR in presence of p-BQ was not significantly decreased with respect to that in absent of scavenger. This indicates that superoxide radical (O_2^-) contributes to a negligible extent towards decolorization process. In addition, the formation of O_2^- by the reduction of O_2 with photo-excited electrons obtained from the conduction band of BFO, is inhibited as the redox potential of O_2/O_2^-(− 0.33 eV) is more negative than the conduction band-edge potential of BFO (+ 0.3 eV) (Zheng et al.). The possibility of participation of electrons in decolorization of CR is also avoided due to a slight decrease of decolorization percentage in presence of DMSO. As shown in Fig. 12a, the percentage of decolorization in presence of IPA and EDTA was significantly decreased as compared to that in absence of scavenger, suggesting the involvement of both hydroxyl radicals and holes in decolorization process.

The presence of hydroxyl radical formation during CR decolorization could be independently verified by fluorescence technique using terephthalic acid (TA) as a sensing probe. The TA traps OH• radical to produce the 2-hydroxyterephthalic acid whose fluorescence intensity can be correlated to the concentration of OH• radicals in water.

$$\bullet OH + TA \rightarrow TAOH$$

The intensity of fluorescence was measured in a 5 × 10–5 M solution of alkaline terephthalic acid in presence of BFO500 catalyst (1 g/L) after 60 min of solar irradiation. The formation of hydroxyl radicals were confirmed by the fluorescence spectra obtained after exciting at 315 nm.

Basing on the above experimental results, a mechanism for BFO-mediated photocatalytic decolorization of CR under solar light irradiation is proposed in Scheme 1, and the mechanistic path way of the whole decolorization process may be described as follows.

BFO500 possessed + 2.1 and + 0.3 eV as valence and conduction band edge potentials respectively with a band gap of 1.8 eV, which corresponds to visible region as evident from UV-Vis DRS spectra. Upon irradiation

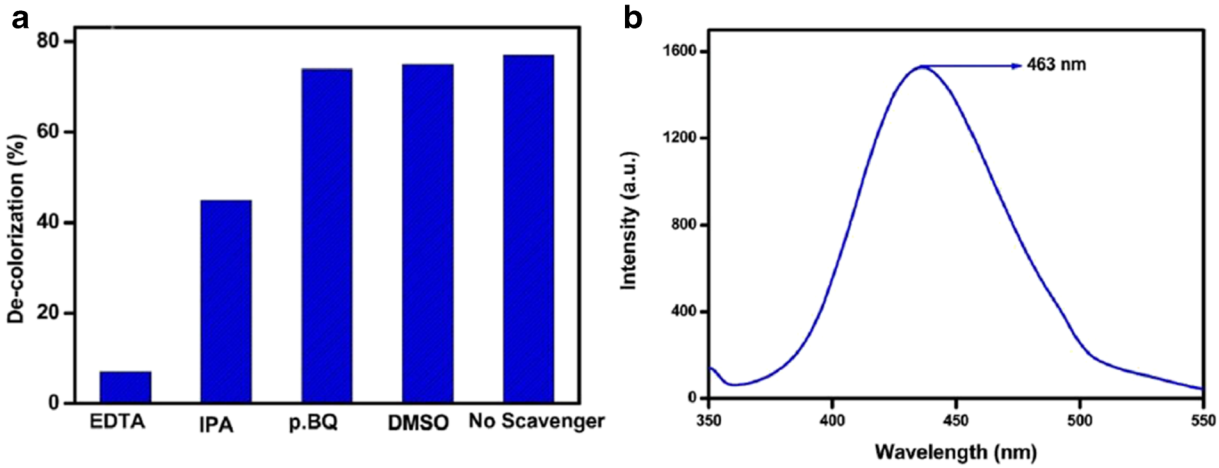

Fig. 12 **a** Effect of scavengers on (%) of photo decolorization of CR using BFO500 photocatalyst. Volume of the solution 20 mL, initial concentration of CR10 mg L^{-1}, irradiation time 60 min, pH 6.5. **b** The fluorescent spectra of 5 × 10–5 M basic solution of 2-hydroxyterephthalic acid confirming the formation of OH• radicals

of solar light, photo-generated electrons and holes are produced at the valence band (VB) and the conduction band (CB) of BFO500, respectively, as shown in Eq. 1. The photo-excited electrons get transferred from the CB of BFO to adsorbed water molecules or nearby water molecules to get solvated. The holes so formed at VB, may decompose the CR molecules directly as represented in Eq. 4 or/and combine with adsorbed water molecules/surface hydroxyl groups to generate hydroxyl free radicals ($OH^{\cdot}$) (Eqs. 5 and 6).The redox potential of OH^{-}/•OH is 1.99 eV which is less positive than the potential of hole on VB of BFO. So, the formation of •OH is directly possible by holes interacting with hydroxyl ion (Zhao et al. 2016). The highly oxidizing •OH free radicals decompose CR molecules (Eq. 7).

$$\mathrm{BFO} + h\vartheta \rightarrow \mathrm{BFO} + (e^{-})\ \mathrm{CB} + (h^{+})\ \mathrm{VB} \quad (3)$$

$$(h^{+})\ \mathrm{VB} + \mathrm{CR\ ads} \rightarrow \mathrm{CR}\ \textit{decolorized} \quad (4)$$

$$(h^{+})\ \mathrm{VB} + \mathrm{H_2O\ ads} \rightarrow \bullet\mathrm{OH} + \mathrm{H^{+}} \quad (5)$$

$$(h^{+})\ \mathrm{VB} + \mathrm{OH^{-}} \rightarrow \bullet\mathrm{OH} \quad (6)$$

$$\bullet\mathrm{OH} + \mathrm{CR\ ads} \rightarrow \mathrm{CR}\ \textit{decolorized} \quad (7)$$

Scheme 1 The proposed mechanism for Congo red decolorization over the BFO500 photocatalyst

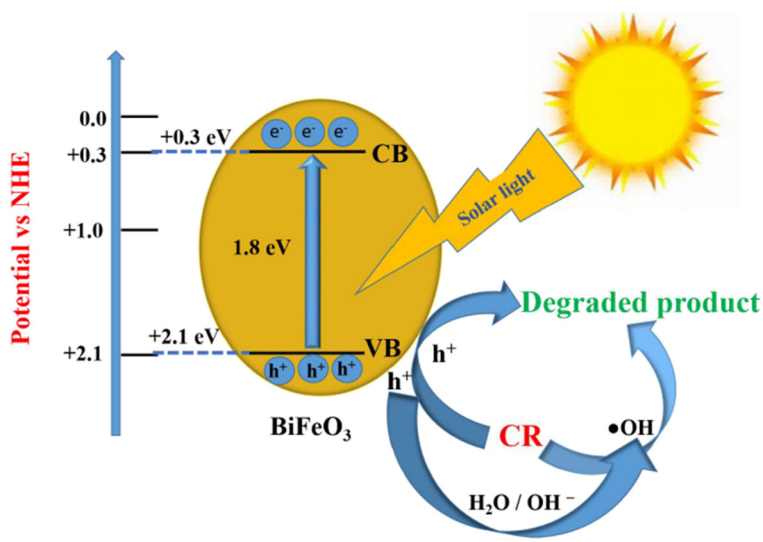

Conclusion

The BFO nanoparticles were synthesized by solid state reaction method and annealed at different temperatures ranging from 350 to 800 °C. The synthesized BFO samples were identified to be polycrystalline in nature and could able to absorb maximum fraction of visible light. Among the synthesized BFO samples, those annealed at 500 °C appeared to be the best photocatalyst for the de-colorization of CR under solar irradiation. This is attributed to high photocurrent generation, low PL intensity implying better charge separation, and low recombination rate, high optical absorption, nanorange particle size (smallest average crystallite size of 30 nm), and better crystallinity. The de-colorization of CR under solar light is primarily due to attack on dye molecules by photo-generated holes and •OH radicals. The multiferroic BFO has exhibited potential for photocatalytic degradation of water-borne pollutants utilizing abundantly available visible portion of solar radiation and may find useful for similar applications towards environmental abetment of pollutants in this context.

Compliance with ethical standards

Conflict of interest The authors declare that they have no conflict of interest.

References

Ahmad M, Mohammad RF, Mohammad RM (2012) Modified Scherrer equation to estimate more accurately nano-crystallite size using XRD. World J Nano Sci Eng 2:154–160

Bai X, Wei J, Tian B, Liu Y, Reiss T, Guiblin N, Gemeiner P, Dkhil B, Infante IC (2016) Size effect on optical and photocatalytic properties in BiFeO3 nanoparticles. J Phys Chem C 120(7): 3595–3601. https://doi.org/10.1021/acs.jpcc.5b09945

Baumanis C, Bahnemann DW (2008) TiO2 thin film electrodes: correlation between photocatalytic activity and electrochemical properties. J Phys ChemC 112:19097–19101

Beranek R (2011) (Photo)electrochemical methods for the determination of the band edge positions of TiO2-based nanomaterials. Adv Phys Chem 2011:1–20. https://doi.org/10.1155/2011/786759

Bharathkumar S, Sakar M, Balakumar S (2016) Experimental evidence for the carrier transportation enhanced visible light driven photocatalytic process in bismuth ferrite (BiFeO3) one-dimensional fiber nanostructures. J Phys Chem C 120(33):18811–18821. https://doi.org/10.1021/acs.jpcc.6b04344

Choi T, Lee S, Choi YJ, Kiryukhin V, Cheong SW (2009) Switchable ferroelectric diode and photovoltaic effect in BiFeO3. Science 324(5923):63–66. https://doi.org/10.1126/science.1168636

Dhanalakshmi R, Muneeswaran M, Vanga PR, Ashok M, Giridharan NV (2016) Enhanced photocatalytic activity of hydrothermally grown BiFeO3 nanostructures and role of catalyst recyclability in photocatalysis based on magnetic framework. Appl Phys A Mater Sci Process 122(1):13–27. https://doi.org/10.1007/s00339-015-9527-z

Gao F, Yuan Y, Wang KF, Chen XY, Chen F, Liu JM, Ren ZF (2006) Preparation and photo absorption characterization of BiFeO3 nanowires. Appl Phys Lett 89(10):102506. https://doi.org/10.1063/1.2345825

Gao F, Chen X, Yin K, Dong S, Ren Z, Yuan F, Yu T, Zou Z, Liu J (2007) Visible- light photocatalytic properties of weak magnetic BiFeO3, nanoparticles. Adv Mater 19(19):2889–2892. https://doi.org/10.1002/adma.200602377

Gao T, Chen Z, Zhu Y, Niu F, Huang Q, Qin L, Sun X, Huang Y (2014) Synthesis of BiFeO3 nanoparticles for the visible-light induced photocatalytic property. Mater Res Bull 59:6–12. https://doi.org/10.1016/j.materresbull.2014.06.022

Giannakopoulou T, Papailias I, Todorova N, Boukos N, Liu Y, Yu J, Trapalis C (2016) Tailoring the energy band gap and edges' potentials of g-C3N4/TiO2 composite photocatalysts for NOx removal. Chem Eng J. https://doi.org/10.1016/j.cej.2015.12.102

Jiang JZ, Zou J, Anjum MN, Yan JC, Huang L, Zhang YX, Chen JF (2011) Synthesis and characterization of wafer-like BiFeO3 with efficient catalytic activity. Solid State Sci 13: 1779–1785

Jing LQ, Zhou W, Tian GH, HG F (2013) Surface tuning for oxide based nanomaterials as efficient photocatalysts. Chem Soc Rev 42(24):9509–9549. https://doi.org/10.1039/c3cs60176e

Joshi UA, Jang JS, Borse PH, Lee JS (2008) Microwave synthesis of single crystalline perovskite BiFeO3 nanocubes for photoelectrode and photocatalytic applications. Appl Phys Lett 92(24):242106. https://doi.org/10.1063/1.2946486

Kandi D, Martha S, Thirumurugan A, Parida KM (2017) Modification of BiOI microplates with CdS QDs for enhancing stability, optical property, electronic behavior toward rhodamine B decolorization and photocatalytic hydrogen evolution. J Phys Chem C 121(9):4834–4849. https://doi.org/10.1021/acs.jpcc.6b11938

Konstantinou IK, Albanis TA (2004) TiO2-assisted photocatalytic degradation of azo dyes in aqueous solution: kinetic and mechanistic investigations: a review. Appl Catal B Env 49(1):1–14. https://doi.org/10.1016/j.apcatb.2003.11.010

Kumar M, Palkar VR, Srinivas K, Suryanarayana SV (2000) Ferroelectricity in a pure BiFeO3 ceramic. Appl Phys Lett 76(19):2764–2766. https://doi.org/10.1063/1.126468

Langford JI, Wilson AJC (1978) Scherrer after sixty years: a survey and some new results in the determination of crystallite size. J Appl Crystallogr 11(2):102–113. https://doi.org/10.1107/S0021889878012844

Li S, Lin Y, Zhang HBP, Wang Y, Nan CW (2010) Controlled fabrication of BiFeO3 uniform microcrystals and their magnetic and photocatalytic behaviours. J Phys Chem C 114(7): 2903–2908. https://doi.org/10.1021/jp910401u

Li D, Guo Y, Hu C, Jiang C, Wang E (2004) Preparation, characterization and photocatalytic property of the $PW_{11}O_{39}^{7-}$/TiO2 composite film towards azo-dye degradation. J Mol Catal 207:181–191

Martha S, Reddy KH, Parida KM, Satapathy PK (2012b) Enhanced photocatalytic activity over N-doped Ga, Zn mixed oxide under visible light irradiation. Intern J Hydro Energ 37(1):115–124. https://doi.org/10.1016/j.ijhydene.2011.09.068

Martha S, Padhi DK, Parida KM (2014a) Reduced graphene oxide/InGaZn mixed oxide nanocomposite photocatalysts for hydrogen production. Chem Sus Chem 7(2):585–597. https://doi.org/10.1002/cssc.201300685

Martha S, Reddy KH, Parida KM (2014b) Fabrication of In2O3 modified ZnO for enhancing stability, optical behaviour, electronic properties and photocatalytic activity for hydrogen production under visible light. J Mater Chem A 2(10):3621–3631. https://doi.org/10.1039/c3ta14285j

Martha S, Reddy KH, Biswal N, Parida KM (2012a) Facile synthesis of InGaZn mixed oxide nanorods for enhanced hydrogen production under visible light. Dalton Trans 41(46):14107–14116. https://doi.org/10.1039/c2dt31949g

McDonnell KA, Wadnerkar N, English NJ, Rahman M, Dowling D (2013) Photo-active and optical properties of bismuth ferrite (BiFeO3): an experimental and theoretical study. Chem Phys Lett 572:78–84. https://doi.org/10.1016/j.cplett.2013.04.024

Moitra D, Ghosh BK, Chandel M, Ghosh NN (2016) Synthesis of BiFeO3 nanowire- reduced graphene oxide based magnetically separable nanocatalyst and its versatile catalytic activity towards multiple organic reactions. RSC Adv 6(100):97941–97952. https://doi.org/10.1039/C6RA22077K

Montazerozohori M, Habibi MH, Joohari S, Khodadostan V (2007) The effects of some operational parameters in photodegradation of benzylamine and aniline and their kinetics in aqueous suspension of Tio2 and Pt–loaded TiO2. Ann Chim 97(10):1015–1026. https://doi.org/10.1002/adic.200790086

Nashim A, Martha S, Parida KM (2013) Gd2Ti2O7/In2O3: efficient visible-light-driven heterojunction-based composite photocatalysts for hydrogen production. Chem Cat Chem 5:2352–2359

Nayak S, Mohapatra L, Parida K (2015) Visible light-driven novel g-C_3N_4/NiFe-LDH composite photocatalyst with enhanced photocatalytic activity towards water oxidation and reduction reaction. J Mater Chem A 36:18622–18635

Nechache R, Harnagea C, Licoccia S, Traversa E, Ruediger A, Pignolet A, Rosei F (2011) Photovoltaic properties of Bi2FeCrO6 epitaxial thin films. Appl Phys Lett 98(20):202902. https://doi.org/10.1063/1.3590270

Patnaik S, Martha S, Madras G, Parida K (2016) The effect of sulfate pretreatment to improve the deposition of Au-nanoparticles in a gold-modified sulfated gC_3N_4 plasmonic photocatalyst towards visible light induced water reduction reaction. Phys Chem Chem Phys 18(41):28502–28514. https://doi.org/10.1039/C6CP04262G

Peng J, Hojamberdiev M, Cao B, Wang J, Xu Y (2011) Surfactant-free hydrothermal synthesis of submicron BiFeO3 powders. Appl Phys A Mater Sci Process 103(2):511–516. https://doi.org/10.1007/s00339-010-6024-2

Quinonez JLO, Dias D, Dbe IZ, Santamaria HA, Betancourt I, Jacinto PS, Etzana NN (2013) Easy synthesis of high-purity BiFeO3 nanoparticles:new insights derived from the structural, optical, and magnetic characterization. Inorg Chem 52(18):10306–10317. https://doi.org/10.1021/ic400627c

Rashad MM (2012) Effect of synthesis conditions on the preparation of BiFeO3 nanopowders using two different methods. J Mater Sci Mater Electron 23(4):882–888. https://doi.org/10.1007/s10854-011-0513-8

Reddy KH, Martha S, Parida KM (2013) Fabrication of novel p-BiOI/n-ZnTiO3 heterojunction for degradation of rhodamine 6G under visible light irradiation. Inorg Chem 52(11):6390–6401. https://doi.org/10.1021/ic400159m

Soltani T, Mohammad HE (2013) Sono-synthesis of bismuth ferrite nanoparticles with high photocatalytic activity in degradation of Rhodamine B under solar light irradiation. Chem Eng J 223:145–154. https://doi.org/10.1016/j.cej.2013.02.124

Soltani T, Entezari MH (2013a) Photolysis and photocatalysis of methylene blue by ferrite bismuth nanoparticles under sunlight irradiation. J Mol Catal A Chem 377:197–203. https://doi.org/10.1016/j.molcata.2013.05.004

Soltani T, Entezari MH (2013b) Solar photocatalytic degradation of RB5 by ferrite bismuth nanoparticles synthesized via ultrasound. Ultrason Sonochem 20(5):1245–1253. https://doi.org/10.1016/j.ultsonch.2013.01.012

Tsai CJ, Yang CY, Liao YC, Chueh YL (2012) Hydrothermally grown bismuth ferrites: controllable phases and morphologies in a mixed KOH/NaOH mineralizer. J Mater Chem 22(34):17432–17436. https://doi.org/10.1039/c2jm33859a

Valant M, Axelsson AK, Alford N (2007) Peculiarities of a solid-state synthesis of multiferroic polycrystalline BiFeO3. Chem Mater 19(22):5431–5436. https://doi.org/10.1021/cm071730+

Wang J, Neaton JB, Zheng H, Nagarajan V, Ogale SB, Liu B, Viehland D, Vaithyanathan V, Schlom DG, Waghmare UV, Spaldin NA, Rabe KM, Wuttig M, Ramesh R (2003) Epitaxial $BiFeO_3$ multiferroic thin film heterostructures. Science 299(5613):1719–1722. https://doi.org/10.1126/science.1080615

Wang X, Lin Y, Ding XF, Jiang JG (2011) Enhanced visible light response photocatalytic activity of bismuth ferrite nanoparticles. J Alloys Comp 509(23):6585–6388. https://doi.org/10.1016/j.jallcom.2011.03.074

Wang YP, Zhou L, Zhang MF, Chen XY, Liu JM, Liu ZG (2004) Room temperature saturated ferroelectric polarization in $BiFeO_3$ ceramics synthesized by rapid liquid phase sintering. Appl Phys Lett 84(10):1731–1733. https://doi.org/10.1063/1.1667612

Zhao Z, Zhang W, Sun Y, Yu J, Zhang Y, Wang H, Dong F, Wu Z (2016) Bi cocatalyst/Bi2MoO6 microspheres nanohybrid with SPR-promoted visible-light photocatalysis. J Phys Chem 120:11889–11898

Zheng L, Zheng Y, Chen C, Zhan Y, Lin X, Zheng Q, Wei K, Zhu J (2009) Network structured SnO_2/ZnO hetero junction nanocatalyst with high photocatalytic activity. J Inorg Chem 48(5):1819–1825. https://doi.org/10.1021/ic802293p